Nanoscale

COMMUNICATION

View Article Online
View Journal

Cite this: DOI: 10.1039/c6nr06300d

Received 8th August 2016,
Accepted 29th September 2016

DOI: 10.1039/c6nr06300d

www.rsc.org/nanoscale

Titania-coated gold nanorods with expanded photocatalytic response. Enzyme-like glucose oxidation under near-infrared illumination†

M. C. Ortega-Liebana,[a,b] J. L. Hueso,*[a,b] R. Arenal[c,d] and J. Santamaria*[a,b]

Gold nanorods coated with a uniform titanium dioxide nanoshell have been prepared and used as glucose-oxidase surrogates. Remarkably, this core–shell photocatalytic nanostructure has been able to induce complete oxidation of glucose at near room temperature (32–34 °C) in a wide range of pH values with the aid of a near-infrared (NIR) irradiation source. In contrast, the uncoated gold nanorods exhibit negligible photo-oxidation response under identical experimental conditions thereby proving the photoactivity of the titania shell towards glucose oxidation. The process takes place *via in situ* photo-generation of singlet oxygen or hydroxyl radicals as reactive oxidative species (ROS). This underlines the role played by the core nanorods as plasmonic light harvesters in the NIR range and constitutes the first example of a NIR-activated enzyme-like catalyst.

The design and development of novel nanostructured materials mimicking the catalytic role of natural enzymes has recently emerged as a promising research field. Enzymes present in natural systems meet a wide variety of appealing requisites as biocatalysts in terms of activity, specificity and high production yields at mild reaction conditions that have sparked the interest of multiple industries (*i.e.* pharmaceutical, food, agrochemical) for the development of specific chemicals.[1–3] Nevertheless, natural enzymes also exhibit some inherent downsides that limit their use for practical applications:[1,2,4] (i) catalytic stability and sensitivity strongly dependent on minimal alterations of their optimal environmental conditions; (ii) difficulties for their recovery and reutilization; (iii) undesired costs derived from the high number of preparation and purification steps required. To circumvent these drawbacks, the search for stable and affordable alternatives has brought the spotlight on the development of artificial enzymatic systems based on inorganic/organic nanomaterials.[1–7]

Different nanostructured materials based on carbon (*i.e.* graphene, carbon nanotubes, carbon dots),[8–10] metals[4,6,7,11–14] (*i.e.* gold, silver, platinum, palladium or alloys), organic–inorganic hybrids[11,15–17] or metal oxides (*i.e.* iron, cobalt, vanadium, ceria)[1,3,18–21] have been recently tested as biomimetic catalysts resembling the activity of peroxidase, dismutase or glucose-oxidase (hereafter GOx) enzymes. The GOx biomimetic systems for glucose oxidation hold a huge potential for biomass conversion, selective detection of glucose at trace levels and control/monitoring of internal metabolism in cells. Much attention has been focused on gold nanoparticles due to their enzyme-mimicking catalytic activity to oxidise glucose into gluconic acid and hydrogen peroxide.[4,6,22] Multiple Au-based configurations have been evaluated by coating NPs with different surface functional groups or by supporting/encapsulating gold onto/within different supports such as ceria or ordered mesoporous supports.[4,8,19,23] The use of mesoporous supports suggested by Lin *et al.*[1,4] paved the way for the direct application of nanoparticles in complex enzymatic process and a dual GOx-like and peroxidase-like behaviour. Alternatively, the use of novel photocatalytic systems inspired in natural photosynthetic centers is also attracting a strong interest.[2,24] Ideally, the whole solar spectrum should be used to facilitate the photo-conversion of glucose,[25,26] prompting the study of semiconductors such as ZnO or TiO_2.[24,27] In this regard, the co-addition of noble-metal based nanoparticles (*i.e.* Au, Pt or Pd) has shown a two-fold positive influence: (i) under UV light irradiation, the presence of small nanoparticles can give rise to enhanced selectivities and to a decrease of the electron–hole recombination rates;[2,24,27] (ii) under visible or even NIR irradiation light, these metals act as light harvesters and sensitizers due to their much larger absorption/scattering

[a]*Institute of Nanoscience of Aragon (INA) and Department of Chemical Engineering and Environmental Technology, University of Zaragoza, 50018 Zaragoza, Spain. E-mail: jesus.santamaria@unizar.es, jlhueso@unizar.es*
[b]*CIBER de Bioingeniería, Biomateriales y Nanomedicina (CIBER-BBN), Centro de Investigación Biomédica en Red, C/Monforte de Lemos 3-5, Pabellón 11, 28029 Madrid, Spain*
[c]*Laboratorio de Microscopías Avanzadas, Instituto de Nanociencia de Aragón, Universidad de Zaragoza, 50018 Zaragoza, Spain*
[d]*ARAID Foundation, 50018 Zaragoza, Spain*

†Electronic supplementary information (ESI) available: Experimental details on the synthesis and characterization of the photocatalyst, kinetics, photocatalytic oxidation experiments and ROS determination. See DOI: 10.1039/c6nr06300d

cross-sections and can inject electrons into the conduction band of semiconductor supports.[2,24,28–36] In particular, the use of gold-based nanostructures with anisotropic shapes has been recently tested as a very appealing alternative for photobiocatalysis.[35–39] Their behaviour is mediated by plasmon resonances that can be exploited to induce highly localized thermal heating, inject hot electrons and enhance the efficiency of light-induced chemical reactions. This work aims at exploring a hybrid Au–TiO_2 photo-catalyst with a core–shell configuration as a glucose-oxidase mimicking inorganic alternative. This hybrid nanostructure combines: (i) a gold nanorod core with excellent NIR absorption capabilities as a plasmonic photo-sensitizer and (ii) a thin titania shell to provide thermal stability and a high photo-activity. The light-induced oxidation of glucose is achieved *via* the *in situ* photo-generation of highly reactive radicals such as singlet oxygen and hydroxyl species. The low thickness of the shell and the high aspect ratio of the core maximize the interface area and the electron transfer efficiency between both phases.

The synthesis of the core plasmonic Au NRs was carried out by the seed-mediated method, combining the use of hexadecyl-trimetylammonium bromide (CTABr) and bromosalicylic acid as stabilizers.[40] Previously reported methods were adapted to obtain an optimum TiO_2 thickness[39,40] (see details in ESI†). To grow a TiO_2 shell surrounding the Au NRs, a ligand exchange with an anionic polymer such as poly-styrene sulfonate (PSS) was first carried out to facilitate contact with the titanium chloride precursor and induce a successful shell growth (see Scheme 1a). ζ-Potential measurements at different pH values confirmed the changes in the net charge for un-coated and titania-coated Au NRs (Fig. S1, ESI†). Furthermore, TEM and high-angle annular dark-field scanning transmission electron microscopy (HAADF-STEM) analysis also corroborated the formation of homogeneous core–shell nanostructures (Fig. 1a–c) with an average length × width: 54 × 16 nm for the Au NRs

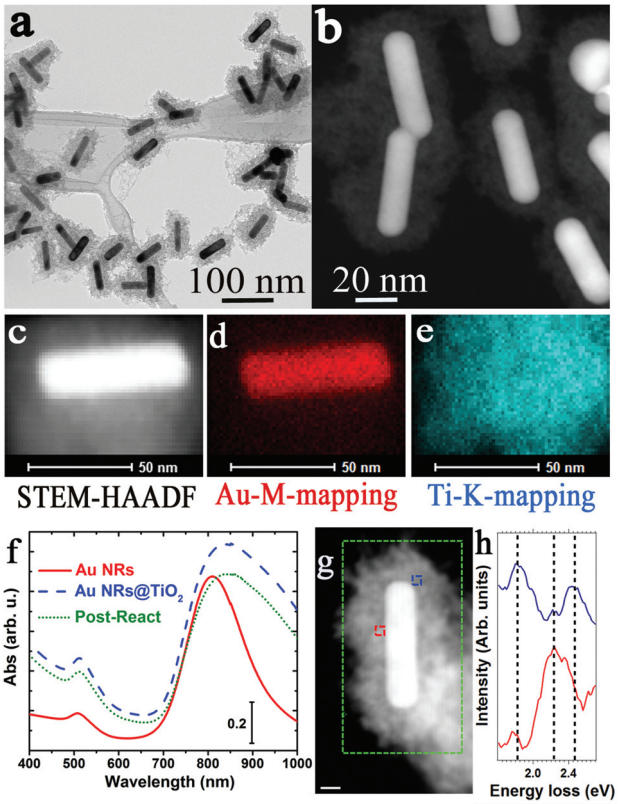

Fig. 1 Characterization of the titania-coated gold nanorods: (a) representative TEM image displaying the homogeneity of the nanostructures; (b) STEM-HAADF image of the hybrid nanostructure accounting for the darker contrast of the TiO_2 shell and the brighter contribution of the gold nanorod in the core; (c–e) EDX elemental mapping distribution of gold (referred to the Au–M edge transition) and titania (referred to Ti-K edge); (f) Absorption spectra with the transversal and longitudinal plasmon resonances of un-coated nanorods and titania-coated gold nanorods before and after photo-catalytic experiments; (g) HAADF-STEM image of an Au nanorod covered by TiO_2. An EELS-SPIM has been acquired in the green marked area (scale bar: 10 nm); (h) EEL spectra (each of them corresponds to the sum of 25 spectra), after removing the zero-loss peak (ZLP), extracted from the EELS-SPIM in the areas marked in g.

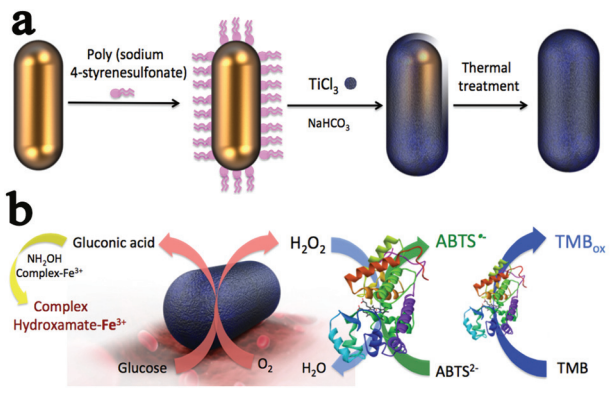

Scheme 1 (a) Scheme of the synthesis steps for titania-coated gold nanorods (see Experimental section for details); (b) schematic description of the colorimetric assays employed to monitor the formation of gluconic acid and hydrogen peroxide as the main reaction products derived from the photo-oxidation of glucose under NIR irradiation at near room temperature (see ESI† for specific details).

(Fig. S2, ESI†). Elemental mapping analysis by Energy-Dispersive X-ray spectroscopy (EDX) clearly defined the presence of gold in the inner part of the nanohybrid composite (Fig. 1d) and an outer shell of TiO_2 (Fig. 1e) with an average thickness of ~14 nm (Fig. S2, ESI†). XRD patterns confirmed that the shell was formed by multiple anatase nanocrystallites (Fig. S3, ESI†). X-ray Photoelectron Spectroscopy (XPS) analysis also supported the formation of a well-oxidized phase of TiO_2 attributed to a binding energy centred at 458.8 eV in the $Ti2p_{3/2}$ photoemission peak (Fig. S4†) and a surface atomic percentage around 100 times higher than gold. Au was mostly identified in its metallic state form at 83 eV in the Au 4f region (Fig. S5†). The optical response of the Au NRs with the addition of the TiO_2 shell was also evaluated by UV-Vis spectroscopy (Fig. 1f).

The longitudinal and transverse plasmon resonances of the original Au NRs were centred at 808 and 532 nm, respectively. Upon TiO_2 coating, the longitudinal plasmon peak was red-shifted towards 850 nm and the maximum broadened in the 850–1000 nm range (Fig. 1f). Similar trends were previously reported by Fang *et al.*[39] and attributed to the modification of the refractive-index in the surrounding medium.[39,41] Fig. 1g displays a low magnification HAADF-STEM image of an Au nanorod coated by TiO_2. High-energy resolution electron energy-loss spectroscopy (HR-EELS)-STEM studies, in the low-loss region (below 50 eV) was performed to locally analyze the optical (plasmonic) response of these nanostructures. This yields highly relevant information of the optical, dielectric and electronic properties of nanomaterials at unprecedented spatial resolution.[42–46] A low-loss EELS spectrum-image (SPIM) has been acquired on the green marked area of this micrograph. From this SPIM-EELS, several spectra have been obtained at different regions, which are highlighted in red and blue. These EEL spectra (each of them corresponding to the sum of 25 spectra), after zero-loss peak (ZLP) subtraction, are plotted in Fig. 1h. The peaks observed in these EEL spectra at ~1.8 eV and 2.2–2.4 eV correspond to local surface plasmons resonances (longitudinal and transverse modes,[47] respectively) of this Au nanorod. It is well established that the LSPR strongly depend on the shape, size and local dielectric environment (TiO_2 coating in this case) of the nanostructure.[43,47–51] These spectra show a slight shift for the transverse mode that is likely related to the TiO_2 sheath. It is worth noting that although the EELS measurements already confirm the absorption measurements, these local analyses are more sensitive to modifications of the plasmonic gold nanorod.

Bare and titania-coated Au NRs were evaluated as photocatalytic enzyme-like glucose oxidase surrogates in the presence of a NIR laser while keeping a constant reaction temperature of 32–34 °C with the aid of a thermostatic bath (Fig. S6 and ESI†). In order to monitor the successful generation of the expected oxidation products (*i.e.* gluconic acid and hydrogen peroxide), different colorimetric assays were carried out over time (see Scheme 1b). First, the formation of gluconic acid was indirectly determined by UV-Vis spectroscopy through the formation of a coloured hydroxamate complex with maximum absorbance intensity at 505 nm in the presence of hydroxylamine and Fe(III) trivalent ions (see Scheme 1b and ESI†). Remarkably, the uncoated AuNRs showed no significant formation of gluconic acid (Fig. 2). In contrast, the photocatalyst with the core–shell configuration progressively converted glucose into gluconic acid as evidenced by the increasing presence of the complex intermediate with maximum absorbance centered at 505 nm (Fig. 2 and S7†). Additional GC-MS analyses further confirmed the conversion of glucose and the progressive formation of gluconic acid and other chemically close acid derivatives (Fig. S8, ESI†). A similar photo-catalytic response could be observed in a broad interval of pH values ranging from 4 to 9, thereby providing this core–shell nano-configuration with a very robust response against pH changes. This is a significant advantage with regards to natural glucose oxidase enzymes that tend to deactivate in non-acidic environments.[4,6] The steady-state rate data were successfully fitted to typical Michaelis-Menten kinetics for the range of glucose concentrations evaluated (Fig. S9 and ESI†). Moreover, a Michaelis constant (K_m) value of ~5.1 mM and a maximum velocity (V_{max}) of 6.7×10^{-6} M s^{-1} were determined for the enzyme-mimicking photo-catalyst. The apparent K_m constant is similar to previously reported values for natural glucose oxidase enzymes or other gold-based artificial nanocatalysts.[4,6] The fact that this core–shell catalyst is selectively activated upon NIR irradiation can be attributed to the photosensitizing role of the Au NR core and expands the photo-response of other Pd/TiO_2 photocatalysts tested in the UV-region.[27] It is also worth mentioning that the present photocatalyst is not only active in a wide range of pH (Fig. S10†) but also exhibits a high thermal stability after multiple laser irradiation cycles (Fig. S11†) that did not affect its plasmonic response in the NIR range (Fig. 1f).

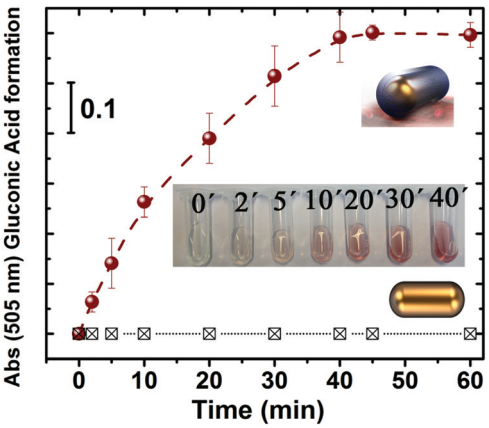

Fig. 2 Comparison of the maximum absorbance intensity detected at 505 nm for the Fe-hydroxamate complex (see also Scheme 1b) formed with the *in situ* generated gluconic acid upon irradiation with a NIR laser at 808 nm at different time intervals and in the presence of the uncoated and titania coated Au NRs, respectively (inset: digital micrographs displaying the characteristic red-color of the complex formed at different reaction times. The un-coated Au NRs exhibited negligible photoactivity and results are not shown); experimental conditions: [glucose] = 10 mM; [catalyst] = 0.02 mg mL^{-1}; pH = 7.4 in 0.2 M NaAc buffer; irradiation experiments with laser wavelength = 808 nm and laser power of 1.5 W; reaction temperature: 33 °C.

The presence of the other main oxidation product (*i.e.* hydrogen peroxide) was tested by two horseradish peroxidase (HRP)-mediated colorimetric assays (Scheme 1b and Fig. S12†). The generated H_2O_2 was subsequently reduced in the presence of the HRP enzyme and induced the simultaneous oxidation of either 2,2-azino-bis (3-ethylbenzothiozoline)-6-sulfonic acid diammonium salt (hereafter ABTS) or 3,3,5,5-tetramethylbenzidine (hereafter TMB) that evolved into coloured dye-derivatives with maximum absorbance intensities at 415 and 652 nm, respectively (Fig. S12†). Again, the uncoated Au NRs showed no evidence of significant photoactivity and only traces of colour were detected in different

assays. In contrast, the titania-coated Au NRs further corroborated their glucose-oxidase mimicking activity by showing an increasing generation of H_2O_2 and the appearance of colorimetric by-products with increasing exposure to NIR irradiation (Fig. S12†), following a similar evolution with respect to the formation of gluconic acid. In order to justify the enhanced photo-catalytic response of the titania-coated Au NRs in comparison with their uncoated counterparts, a series of reactivity tests were performed to confirm the *in situ* generation of reactive oxidative species, responsible for the oxidation of glucose both in the absence (Fig. S13†) and in the presence of plasmonic resonance conditions. Firstly, the generation of singlet oxygen $^1O_2$, a highly reactive oxygen species typically involved in photo-catalytic events, was monitored using 9,10-anthracenediyl-bis(methylene) dimalonic acid (ABDA) as molecular probe. ABDA reacts with $^1O_2$ to yield an endoperoxide (Fig. 3a), causing a reduction in the absorption intensity of the anthracene core of the probe. This decrease in the absorption spectra of ABDA was drastically accelerated for the titania-coated photo-catalyst as shown in Fig. 3b and c, respectively. In addition, the formation of highly reactive hydroxyl radicals ($^{\bullet}OH$) was also systematically evaluated with the aid of disodium terephthalate (NaTA) that selectively reacts with $^{\bullet}OH$ radical groups to form 2-hydroxy disodium terephthalate, a fluorescent compound emitting at 425 nm (Fig. 3d). Indeed, the progressive formation of hydroxyl groups upon NIR illumination was detected in the presence of both the uncoated (Fig. 3e) and especially for the titania-coated Au NRs that favoured an approximately 3-times stronger fluorescence emission (Fig. 3f). In the absence of a NIR illumination source, no evidence of radical formation was detected (Fig. S14†). These results further explain the obtained photo-catalytic activity obtained under NIR irradiation and the efficient response of the Au NRs when surrounded by a homogeneous titania shell. While the resonant plasmon excitation of the un-coated Au NRs under NIR illumination is evident, it becomes clear that the efficiency of the electron transfer mechanism to induce ROS and promote the photo-oxidation of glucose is poorer with bare Au NRs than in the case of the core–shell configuration with titania. Additional control experiments in the absence of NIR illumination also confirmed the photo-activation pre-requirements to promote the glucose transformation (Fig. S14†). Previous reports on Au-based catalysts have shown the critical influence of the chemical nature of the ligands attached to the gold surface to obtain an efficient catalytic response towards glucose oxidation. Therefore, the CTABr bilayer that is typically used to direct synthesis and stabilize Au NRs may have a detrimental effect, hindering the interaction with the reactant molecules, glucose in this case. In contrast, the replacement of CTABr by a TiO_2 continuous shell induces the effective formation of a Schottky barrier at the interface between Au and TiO_2 that, under plasmon excitation conditions, would favour the generation of a population of electron–hole pairs.[39] Subsequently, a fraction of the excited electrons present at energy levels higher than the Schottky barrier (*i.e.* hot electrons) would be injected into the conduction band of TiO_2 (Fig. S15†). These injected electrons can subsequently interact with surrounding oxygen molecules to form superoxide anion radicals[39,52] ($O_2^{\bullet-}$) that readily react to yield singlet oxygen[39,53–55] ($^1O_2$) or hydroxyl radicals[39,53–55] ($^{\bullet}OH$), respectively as depicted in Fig. S15.† These ROS generation routes seem the most plausible, given the high reactivity and short-lived stability of superoxide anion radical and the results obtained with ABDA and NaTA, respectively (Fig. 3 and S13–S15†).

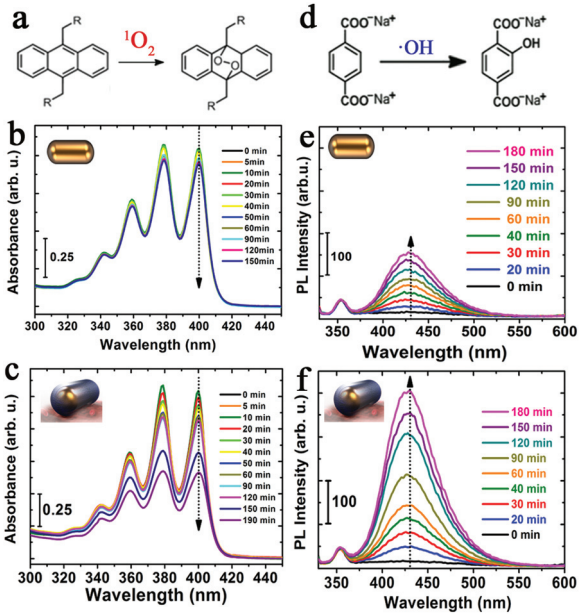

Fig. 3 (a) Structure of ABDA and specific reaction with the *in situ* generated singlet oxygen species; (b) time-dependent absorption spectra evolution of ABDA in the presence of uncoated AuNRs at different NIR irradiation times; (c) time-dependent absorption spectra evolution of ABDA in the presence of titania-coated AuNRs at different NIR irradiation times; (d) specific reaction between the *in situ* generated hydroxyl radicals and NaTA to generate a fluorescent derivative; (e) fluorescence spectra of the different solutions of the NaTA hydroxylated derivative at different irradiation times in the presence of uncoated AuNRs; (f) fluorescence spectra of the different solutions of the NaTA hydroxylated derivative in the presence of titania-coated AuNRs at different NIR irradiation times. Experimental details: [catalyst] = 0.02 mg mL^{-1}; pH = 7.4 in 0.2 M NaAc buffer; laser wavelength = 808 nm; laser power = 1.5 W; reaction temperature: 19–20 °C; [ABDA] = 0.12 mM; [NaTA] = 5 mM; specific dilutions and the generation of NaTA are further described in the ESI.†

In summary, the hybrid nanostructure formed by Au nanorods surrounded by an anatase shell presents exciting possibilities as the first example of a NIR activated enzyme-like catalyst. This structure might be also potentially applied in the visible and UV range, given the UV-photoactive response of titania and the expected sensitizing effect stemming from the transversal modes in the plasmonic Au nanorods. Potential applications range from biomass conversion, (by expanding the photo-response of photocatalysts towards the whole UV-Vis-NIR range) to medical devices for the control of glucose levels, by taking advantage of the deeper penetration of NIR light.

Acknowledgements

The (S)TEM and EELS studies were conducted at the Laboratorio de Microscopias Avanzadas, Instituto de Nanociencia de Aragon, Universidad de, Spain. The authors acknowledge the European Research Council for funding through an advanced grant research project (HECTOR grant number 267626) and a CIG-Marie Curie Reintegration Grant (NANOLIGHT REA grant number 294094). The syntheses of materials have been performed by the Platform of Production of Biomaterials and Nanoparticles of the NANOBIOSIS ICTS, more specifically by the Nanoparticle Synthesis Unit of the CIBER in BioEngineering, Biomaterials & Nanomedicine (CIBER-BBN). Some of the research leading to these results has received funding from the European Union Seventh Framework Programme under Grant Agreement 312483-ESTEEM2 (Integrated Infrastructure Initiative – I3). R.A. gratefully acknowledges the support from the Spanish Ministerio de Economia y Competitividad (FIS2013-46159-C3-3-P) and from the European Union H2020 program ETN project "Enabling Excellence" Grant Agreement 642742. M.C.O. also acknowledges the Spanish Government for the receipt of an FPU predoctoral grant. The authors also thank Dr Bueno-Alejo for helpful discussions of the results.

Notes and references

1 Y. H. Lin, J. S. Ren and X. G. Qu, *Acc. Chem. Res.*, 2014, **47**, 1097–1105.
2 J. A. Macia-Agullo, A. Corma and H. Garcia, *Chem. – Eur. J.*, 2015, **21**, 10940–10959.
3 H. Wei and E. K. Wang, *Chem. Soc. Rev.*, 2013, **42**, 6060–6093.
4 Y. H. Lin, Z. H. Li, Z. W. Chen, J. S. Ren and X. G. Qu, *Biomaterials*, 2013, **34**, 2600–2610.
5 P. F. Zhan, Z. G. Wang, N. Li and B. Q. Ding, *ACS Catal.*, 2015, **5**, 1489–1498.
6 W. J. Luo, C. F. Zhu, S. Su, D. Li, Y. He, Q. Huang and C. H. Fan, *ACS Nano*, 2010, **4**, 7451–7458.
7 X. H. Xia, J. T. Zhang, N. Lu, M. J. Kim, K. Ghale, Y. Xu, E. McKenzie, J. B. Liu and H. H. Yet, *ACS Nano*, 2015, **9**, 9994–10004.
8 P. Y. Qi, S. S. Chen, J. Chen, J. W. Zheng, X. L. Zheng and Y. Z. Yuan, *ACS Catal.*, 2015, **5**, 2659–2670.
9 W. B. Shi, Q. L. Wang, Y. J. Long, Z. L. Cheng, S. H. Chen, H. Z. Zheng and Y. M. Huang, *Chem. Commun.*, 2011, **47**, 6695–6697.
10 E. Gonzalez-Dominguez, M. Comesana-Hermo, R. Marino-Fernandez, B. Rodriguez-Gonzalez, R. Arenal, V. Salgueirino, D. Moldes, A. M. Othman, M. Perez-Lorenzo and M. A. Correa-Duarte, *ChemCatChem*, 2016, **8**, 1264–1268.
11 X. M. Chen, X. T. Tian, B. Y. Su, Z. Y. Huang, X. Chen and M. Oyama, *Dalton Trans.*, 2014, **43**, 7449–7454.
12 J. Li, M. M. Lu, Z. N. Tan, Y. B. Xu, Y. C. Zhang, X. Y. Hu and Z. J. Yang, *Microchim. Acta*, 2016, **183**, 1705–1712.
13 X. Jin, M. Zhao, J. Shen, W. J. Yan, L. M. He, P. S. Thapa, S. Q. Ren, B. Subramaniam and R. V. Chaudhari, *J. Catal.*, 2015, **330**, 323–329.
14 S. Hermans and M. Devillers, *Appl. Catal., A*, 2002, **235**, 253–264.
15 N. Toshima and H. J. Zhang, *Macromol. Symp.*, 2012, **317**, 149–159.
16 Y. Y. Huang, X. Ran, Y. H. Lin, J. S. Ren and X. G. Qu, *Chem. Commun.*, 2015, **51**, 4386–4389.
17 T. Ishida, K. Kuroda, N. Kinoshita, W. Minagawa and M. Haruta, *J. Colloid Interface Sci.*, 2008, **323**, 105–111.
18 H. M. Jia, D. F. Yang, X. N. Han, J. H. Cai, H. Y. Liu and W. W. He, *Nanoscale*, 2016, **8**, 5938–5945.
19 N. J. Lang, B. W. Liu and J. W. Liu, *J. Colloid Interface Sci.*, 2014, **428**, 78–83.
20 X. Jin, M. Zhao, W. J. Yan, C. Zeng, P. Bobba, P. S. Thapa, B. Subramaniam and R. V. Chaudhari, *J. Catal.*, 2016, **337**, 272–283.
21 Y. Y. Huang, Z. Liu, C. Q. Liu, E. G. Ju, Y. Zhang, J. S. Ren and X. G. Qu, *Angew. Chem., Int. Ed.*, 2016, **55**, 6645–6649.
22 M. Comotti, C. Della Pina, E. Falletta and M. Rossi, *Adv. Synth. Catal.*, 2006, **348**, 313–316.
23 A. Mayoral, R. Arenal, V. Gascon, C. Marquez-Alvarez, R. M. Blanco and I. Diaz, *ChemCatChem*, 2013, **5**, 903–909.
24 A. Primo, A. Corma and H. Garcia, *Phys. Chem. Chem. Phys.*, 2011, **13**, 886–910.
25 E. Nikolla, Y. Roman-Leshkov, M. Moliner and M. E. Davis, *ACS Catal.*, 2011, **1**, 408–410.
26 M. Moliner, Y. Roman-Leshkov and M. E. Davis, *Proc. Natl. Acad. Sci. U. S. A.*, 2010, **107**, 6164–6168.
27 B. W. Zhou, J. L. Song, H. C. Zhou, T. B. Wu and B. X. Han, *Chem. Sci.*, 2016, **7**, 463–468.
28 J. Chen, J. Cen, X. L. Xu and X. N. Li, *Catal. Sci. Technol.*, 2016, **6**, 349–362.
29 G. Zhang, G. Kim and W. Choi, *Energy Environ. Sci.*, 2014, **7**, 954–966.
30 C. L. Wang and D. Astruc, *Chem. Soc. Rev.*, 2014, **43**, 7188–7216.
31 S. Sarina, E. R. Waclawik and H. Y. Zhu, *Green Chem.*, 2013, **15**, 1814–1833.
32 S. Linic, P. Christopher and D. B. Ingram, *Nat. Mater.*, 2011, **10**, 911–921.
33 L. Gomez, V. Sebastian, M. Arruebo, J. Santamaria and S. B. Cronin, *Phys. Chem. Chem. Phys.*, 2014, **16**, 15111–15116.
34 A. Pineda, L. Gomez, A. M. Balu, V. Sebastian, M. Ojeda, M. Arruebo, A. A. Romero, J. Santamaria and R. Luque, *Green Chem.*, 2013, **15**, 2043–2049.
35 H. F. Cheng, K. Fuku, Y. Kuwahara, K. Mori and H. Yamashita, *J. Mater. Chem. A*, 2015, **3**, 5244–5258.
36 J. B. Cui, Y. J. Li, L. Liu, L. Chen, J. Xu, J. W. Ma, G. Fang, E. B. Zhu, H. Wu, L. X. Zhao, L. Y. Wang and Y. Huang, *Nano Lett.*, 2015, **15**, 6295–6301.

37 A. Sanchez-Iglesias, A. Chuvilin and M. Grzelczak, *Chem. Commun.*, 2015, **51**, 5330–5333.
38 A. Sanchez-Iglesias, J. Barroso, D. M. Solis, J. M. Taboada, F. Obelleiro, V. Pavlov, A. Chuvilin and M. Grzelczak, *J. Mater. Chem. A*, 2016, **4**, 7045–7052.
39 C. H. Fang, H. L. Jia, S. Chang, Q. F. Ruan, P. Wang, T. Chen and J. F. Wang, *Energy Environ. Sci.*, 2014, **7**, 3431–3438.
40 Z. K. Zheng, T. Tachikawa and T. Majima, *J. Am. Chem. Soc.*, 2015, **137**, 948–957.
41 Q. F. Ruan, C. H. Fang, R. B. Jiang, H. L. Jia, Y. H. Lai, J. F. Wang and H. Q. Lin, *Nanoscale*, 2016, **8**, 6514–6526.
42 J. Nelayah, M. Kociak, O. Stephan, F. J. G. de Abajo, M. Tence, L. Henrard, D. Taverna, I. Pastoriza-Santos, L. M. Liz-Marzan and C. Colliex, *Nat. Phys.*, 2007, **3**, 348–353.
43 M. Bosman, V. J. Keast, M. Watanabe, A. I. Maaroof and M. B. Cortie, *Nanotechnology*, 2007, 18.
44 M. Prieto, R. Arenal, L. Henrard, L. Gomez, V. Sebastian and M. Arruebo, *J. Phys. Chem. C*, 2014, **118**, 28804–28811.
45 R. Arenal, X. Blase and A. Loiseau, *Adv. Phys.*, 2010, **59**, 101–179.
46 R. Arenal, O. Stephan, M. Kociak, D. Taverna, A. Loiseau and C. Colliex, *Phys. Rev. Lett.*, 2005, **95**, 127601.
47 M. N'Gom, S. Z. Li, G. Schatz, R. Erni, A. Agarwal, N. Kotov and T. B. Norris, *Phys. Rev. B: Condens. Matter*, 2009, **80**, 113411.
48 L. Novotny and B. Hecht, *Principles of Nano-Optics*, Cambridge Univ. Press, 2006.
49 S. A. Maier, *Plasmonics: Fundamentals and Applications*, Springer, 2007.
50 R. Arenal, L. Henrard, L. Roiban, O. Ersen, J. Burgin and M. Treguer-Delapierre, *J. Phys. Chem. C*, 2014, **118**, 25643–25650.
51 M. Kociak and O. Stephan, *Chem. Soc. Rev.*, 2014, **43**, 3865–3883.
52 M. Hayyan, M. A. Hashim and I. M. AlNashef, *Chem. Rev.*, 2016, **116**, 3029–3085.
53 B. I. Kruft and A. Greer, *Photochem. Photobiol.*, 2011, **87**, 1204–1213.
54 A. Greer, *Acc. Chem. Res.*, 2006, **39**, 797–804.
55 C. Schweitzer and R. Schmidt, *Chem. Rev.*, 2003, **103**, 1685–1757.

